



**HAL**  
open science

## Alteration of birnessite reactivity in dynamic anoxic/oxic environments

Qinzhi Li, Dieter Schild, Mathieu Pasturel, Johannes L Lützenkirchen, Khalil  
Hanna

► **To cite this version:**

Qinzhi Li, Dieter Schild, Mathieu Pasturel, Johannes L Lützenkirchen, Khalil Hanna. Alteration of birnessite reactivity in dynamic anoxic/oxic environments. *Journal of Hazardous Materials*, 2022, 433, pp.128739. 10.1016/j.jhazmat.2022.128739 . hal-03632132

**HAL Id: hal-03632132**

**<https://hal.science/hal-03632132v1>**

Submitted on 9 Feb 2023

**HAL** is a multi-disciplinary open access archive for the deposit and dissemination of scientific research documents, whether they are published or not. The documents may come from teaching and research institutions in France or abroad, or from public or private research centers.

L'archive ouverte pluridisciplinaire **HAL**, est destinée au dépôt et à la diffusion de documents scientifiques de niveau recherche, publiés ou non, émanant des établissements d'enseignement et de recherche français ou étrangers, des laboratoires publics ou privés.

1           **Alteration of Birnessite Reactivity in Dynamic Anoxic/Oxic**

2                                   **Environments**

3  
4           Qinzhi Li<sup>a</sup>, Dieter Schild<sup>b</sup>, Mathieu Pasturel<sup>c</sup>, Johannes Lützenkirchen<sup>b</sup>, and Khalil  
5                                   Hanna<sup>a,d,\*</sup>

6  
7           <sup>a</sup>*Univ Rennes, École Nationale Supérieure de Chimie de Rennes, CNRS, ISCR –*  
8                                   *UMR6226, F-35000 Rennes, France*

9           <sup>b</sup>*Institute for Nuclear Waste Disposal (INE), Karlsruhe Institute of Technology (KIT),*  
10                                   *P.O. 3640, D-76021 Karlsruhe, Germany.*

11           <sup>c</sup>*Univ. Rennes, CNRS, ISCR – UMR 6226, F-35000, Rennes, France*

12           <sup>d</sup>*Institut Universitaire de France (IUF), MESRI, 1 rue Descartes, 75231 Paris, France.*

13  
14  
15  
16           \*Corresponding author: K Hanna, +33 2 23 23 80 27; [khalil.hanna@ensc-rennes.fr](mailto:khalil.hanna@ensc-rennes.fr)

17  
18  
19

20 **Abstract**

21 Although the oxidative capacity of manganese oxides has been widely investigated,  
22 potential changes of the surface reactivity in dynamic anoxic/oxic environments have  
23 been often overlooked. In this study, we showed that the reactivity of layer structured  
24 manganese oxide (birnessite) was highly sensitive to variable redox conditions within  
25 environmentally relevant ranges of pH (4.0 – 8.0), ionic strength (0 to 100 mM NaCl)  
26 and Mn(II)/MnO<sub>2</sub> molar ratio (0 - 0.58) using ofloxacin (OFL), a typical antibiotic, as  
27 a target contaminant. In oxic conditions, OFL removal was enhanced relative to anoxic  
28 environments under alkaline conditions. Surface-catalyzed oxidation of Mn(II) enabled  
29 the formation of more reactive Mn(III) sites for OFL oxidation. However, an increase  
30 in Mn(II)/MnO<sub>2</sub> molar ratio suppressed MnO<sub>2</sub> reactivity, probably because of  
31 competitive binding between Mn(II) and OFL and/or modification in MnO<sub>2</sub> surface  
32 charge. Monovalent cations (*e.g.*, Na<sup>+</sup>) may compensate the charge deficiency caused  
33 by the presence of Mn(III), and affect the aggregation of MnO<sub>2</sub> particles, particularly  
34 under oxic conditions. An enhancement in the removal efficiency of OFL was then  
35 confirmed in the dynamic two-step anoxic/oxic process, which emulates oscillating  
36 redox conditions in environmental settings. These findings call for a thorough  
37 examination of the reactivity changes at environmental mineral surfaces (*e.g.*, MnO<sub>2</sub>)  
38 in natural systems that may be subjected to alternation between anaerobic and  
39 oxygenated conditions.

40 **Keywords:** manganese oxide; redox; antibiotics; oxidation; removal.

41

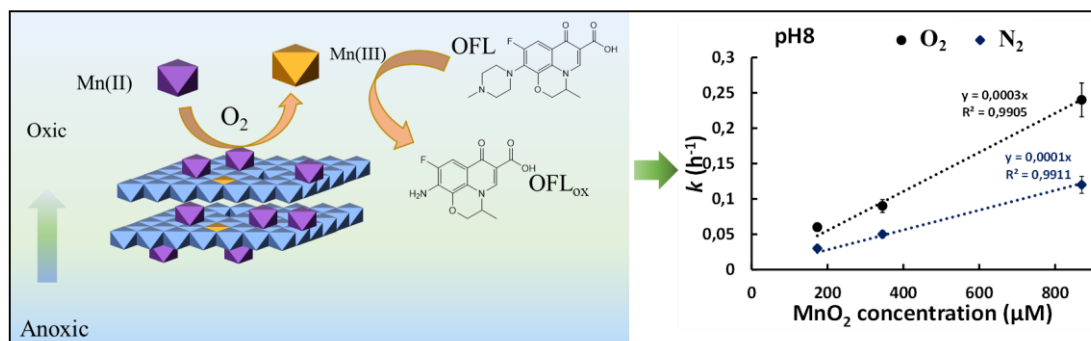
## Table of contents

42

Surface-catalyzed oxidation of Mn(II) by dissolved oxygen controls the reactivity of

43

nanostructured birnessite.



44

45

46 **1. Introduction**

47 Manganese dioxides ( $\text{MnO}_2$ ) are ubiquitous in a wide range of aquatic and terrestrial  
48 environments (Post, 1999). They are widely used in various energy and environmental  
49 applications, because of their specific nanoscale properties, high surface areas, low cost,  
50 strong oxidation and sorption abilities (Post, 1999; Remucal and Ginder-Vogel, 2014).  
51 The layer structured manganese oxide (*e.g.*, birnessite) is structurally similar to  
52 biogenically precipitated natural manganese oxides, and thus the common natural  
53 occurring  $\text{MnO}_2$  in surficial environments. It basically consists of randomly stacked  
54 edge-sharing  $\text{MnO}_6$  octahedra and has a large excess of negative charges because of the  
55 Mn(IV) vacancies and substitution of Mn(II)/(III) for Mn(IV) (Elzinga, 2011). As a  
56 result,  $\text{MnO}_2$  exhibits a high affinity for cation sorption, but also a non-negligible anion  
57 adsorption capacity. Another important feature of  $\text{MnO}_2$  is the ease of switching the  
58 oxidation state, which imparts a good catalytic activity (Post, 1999; Remucal and  
59 Ginder-Vogel, 2014).

60 In oxic environments, it has been reported that  $\text{MnO}_2$  surfaces can catalyze the  
61 oxidation of Mn(II) by dissolved oxygen to generate Mn(III)/(IV) (Yang et al., 2018;  
62 Zhao et al., 2016), while homogeneous oxidation of Mn(II) by oxygen is considered  
63 kinetically sluggish (Davies and James, 1989; Diem et al., 1984; Lan et al., 2017; Nico  
64 et al., 2002; Wilson, 1980). Surface oxygen ligands bound to inner-sphere adsorbed  
65 Mn(II) may accelerate the electron transfer between Mn(II) and  $\text{O}_2$  (Junta and Hochella,  
66 1994; Lan et al., 2017; Luther, 2005; Namgung et al., 2020), leading to higher Mn(II)  
67 removal under oxic conditions compare to anoxic conditions at circumneutral to

68 alkaline pH (Elzinga, 2011; Lefkowitz et al., 2013; Li et al., 2020). The accumulated  
69 Mn(III) can incorporate into Mn octahedral layers and induce the transformation of  
70 MnO<sub>2</sub> (Hinkle et al., 2017; Wang et al., 2018a).

71 Although the influence of phase transformation on the reactivity of birnessite has been  
72 already investigated (Lefkowitz and Elzinga, 2015; Wang et al., 2018a; Wang et al.,  
73 2019), very little knowledge exists about the impact of oxygen on the removal of  
74 organic compounds interacted with MnO<sub>2</sub> surfaces. Furthermore, MnO<sub>2</sub> may co-exist  
75 with dissolved Mn(II) and emerging contaminants in natural systems which may be  
76 subjected to alternation between anaerobic and oxic conditions, such as water-sediment  
77 interfaces, water table fluctuations, groundwater recharge (Jeong et al., 2010; Wu et al.,  
78 2020; Zhao et al., 2021). However, little is known about the potential changes in the  
79 surface reactivity of MnO<sub>2</sub> in environmental settings under alternating redox conditions.  
80 This work has examined for the first time how a shift of redox conditions from anoxic  
81 into oxic may alter the reactivity of birnessite.

82 Ofloxacin (OFL) was chosen here as a target contaminant in order to explore the  
83 changes in MnO<sub>2</sub> reactivity under dynamic anoxic/oxic conditions. OFL is widely used  
84 in human and veterinary medicine, and frequently detected in surface water,  
85 groundwater, soils and municipal wastewater systems, with concentration ranging from  
86 ng/L to µg/L (Zhang and Huang, 2005). Removal kinetics of OFL in the presence of  
87 acid birnessite were performed at pH ranging from 4.0 to 8.0, representing the common  
88 pH conditions of suboxic environments (Elzinga, 2016; Wang et al., 2018a). The  
89 oxidation byproducts of OFL were determined using an ultra performance liquid

90 chromatography-tandem mass spectrometry (UPLC-MS/MS). The oxidative capacity  
91 of MnO<sub>2</sub> was further monitored for variable Mn(II)/MnO<sub>2</sub> molar ratios and ionic  
92 strengths under environmentally relevant conditions. In addition, X-ray diffraction  
93 (XRD), X-ray photoelectron spectroscopy (XPS) and scanning electron microscopy  
94 (SEM) were used to identify the changes in Mn valence states and mineral phase  
95 transformation. This work calls for more consideration of alteration of the oxidative  
96 capacity of birnessite in redox transition zone in groundwater systems.

97

## 98 **2. Materials and Methods**

### 99 **2.1. Materials and Chemicals**

100 All chemicals employed in this study were purchased from Sigma-Aldrich of analytical  
101 grade and used without further purification. Ultrapure water (specific resistivity, 18.2  
102 MΩ cm<sup>-1</sup>, Milli-Q, Millipore) was used for all solutions and suspensions.

103 Acid birnessite was synthesized by reacting KMnO<sub>4</sub> and HCl as described in previous  
104 studies (Li et al., 2020; Mckenzie, 1971; Pokharel et al., 2020). The purity of mineral  
105 phase was confirmed with XRD and SEM (Figure S1). The specific surface area (SSA)  
106 measured by Brunauer-Emmett-Teller (BET)-N<sub>2</sub> adsorption was 85.0 ± 3.0 m<sup>2</sup> g<sup>-1</sup> and  
107 the isoelectric point (pH<sub>IEP</sub>) was around 2.0, respectively (Figure S2). Analysis of XPS  
108 data showed that the average oxidation state of the pristine material was 3.87, with 88.3 %  
109 Mn(IV), 10.7 % Mn(III) and 1.0 % Mn(II) (Figure S3).

### 110 **2.2. Batch experiments**

111 All batch experiments were carried out in 500 mL polyethylene bottles, containing

112 varying concentrations of acid birnessite. The solutions were spiked with aliquots of  
113 1.0 mM OFL and 0.05 M  $\text{MnCl}_2$  stock solution to achieve initial concentration of 10  
114  $\mu\text{M}$  OFL and variable target  $\text{Mn(II)}$  concentrations ranging from 0 to 200  $\mu\text{M}$ . The ionic  
115 strength was fixed using NaCl at various concentrations. The pH of the suspensions  
116 was adjusted to the desired values over the reaction time using an auto pH titrator with  
117 addition of small volumes of HCl (0.1 M) or NaOH (0.1 M) solutions and maintained  
118 at pH 4.0, 6.0 and 8.0 throughout the experiments. No pH buffers were used, to prevent  
119 any impact on the birnessite reactivity. The stirring speed of the mixture was maintained  
120 at 350 rpm. Batch experiments were carried out under ambient air atmosphere or by  
121 bubbling oxygen gas (oxic conditions), or by bubbling nitrogen gas (anoxic conditions).  
122 A two-step anoxic/oxic dynamic process was investigated as follows: after a period of  
123 anoxic conditions where the bottle was under  $\text{N}_2$ , an oxic environment was  
124 subsequently created by removing the cap of the bottle or by bubbling  $\text{O}_2$ . The same  
125 kinetic behavior was observed when either the suspension was stirred under open  
126 atmosphere (ambient air) or with bubbling  $\text{O}_2$  (data not shown). In the open system,  
127  $\text{CO}_2$  from the atmosphere will generate carbonates in solution at high pH values, but  
128 this effect on the reactivity can be excluded according to a previous study (Li et al.,  
129 2020).

130 Aliquots of solution were periodically withdrawn and filtered through a 0.20  $\mu\text{m}$   
131 membrane filter for analysis of OFL concentration, whereas other aliquots without  
132 filtration were immediately mixed with 0.1 M ascorbic acid to quench the reaction. At  
133 the end of experiments, the remaining suspensions were centrifuged at 4500 rpm for 20



134 min and settled particles were freeze-dried, and then stored at 4 °C for further solid  
135 analysis. In another experimental series involving mixing with 1.0 mM sodium  
136 pyrophosphate, a volume of about 3.0 mL sample was periodically withdrawn from the  
137 mixed solution, filtered and analyzed immediately by UV–Vis spectrophotometry in  
138 the range of 200-600 nm wavelength. Batch experiments were conducted in triplicates  
139 and the standard deviation was calculated for each experimental series.

### 140 **2.3. Analytical methods**

141 The concentration of OFL in the samples was analyzed via High Performance Liquid  
142 Chromatography analysis with UV–Vis detection (HPLC-UV) equipped with a  
143 reversed-phase C18 column (250 mm × 4.6 mm i.d., 5 μm) and a UV–Vis detector  
144 (Waters 2489) at a wavelength of 287 nm. The mobile phase consisted of  
145 acetonitrile/water (15/85 v/v,) containing 0.1% formic acid at a flow rate of 0.6 mL/min.  
146 Filtered suspensions were digested with 2% nitric acid and dissolved Mn(II)  
147 concentrations were determined by Atomic Absorption Spectroscopy (AAS, AA140,  
148 Varian, Shimadzu) with a detection limit of 0.02 μM.

149 The oxidation byproducts of OFL were identified using an ultra performance liquid  
150 chromatography-tandem mass spectrometry (UPLC-MS/MS) system. An electrospray  
151 interface was used for the MS measurements in positive ionisation mode and full scan  
152 acquisition.

153 XPS spectra were recorded on an XPS system PHI 5000 VersaProbe II (ULVAC-PHI  
154 Inc.) equipped with a scanning microprobe X-ray source (monochromatic Al K $\alpha$ ,  $h\nu =$   
155 1486.7 eV). An electron flood gun generating low energy electrons (1.1 eV) and low

156 energy argon ions (6 eV) by a floating ion gun were applied for charge compensation  
157 at isolating samples (dual beam technique). Survey scans were recorded with an X-ray  
158 source power of 31 W, X-ray spot size diameter 200  $\mu\text{m}$ , and pass energy of the analyzer  
159 of 187.85 eV. Narrow scans of the elemental lines were recorded at 23.5 eV pass energy,  
160 which yields an energy resolution of 0.69 eV FWHM at the Ag 3d<sub>5/2</sub> elemental line of  
161 pure silver. Calibration of the binding energy scale of the spectrometer was performed  
162 using well-established binding energies of elemental lines of pure metals  
163 (monochromatic Al K $\alpha$ : Cu 2p<sub>3/2</sub> at 932.62 eV, Au 4f<sub>7/2</sub> at 83.96 eV) (Seah et al., 1998).  
164 The error in binding energies of elemental lines is estimated to  $\pm 0.1$  eV for conductors  
165 and  $\pm 0.2$  eV for isolating samples. High-resolution XPS spectra were calibrated by the  
166 carbon deposit C1s binding energy at 284.8 eV and further analyzed by CasaXPS  
167 software. After Shirley background subtractions, all peaks were fitted using 70:30  
168 Gaussian: Lorentzian sum function.

169 A FEI Quanta 650 FEG environmental scanning electron microscope (now Thermo  
170 Fisher Scientific Inc.) was applied to image the sample surfaces.

171 XRD data were collected by using a D8 Advance (Bruker) diffractometer with Cu K $\alpha$   
172 radiation over the range of 10–80° 2 $\theta$  at a step size of 0.02° and phases were determined  
173 according to the PDF database in Jade 6 software.

174

### 175 **3. Results and Discussion**

#### 176 **3.1. Effect of oxygen and pH on the initial removal rate of OFL by MnO<sub>2</sub>**

177 Removal kinetics of OFL were investigated under anoxic and oxic conditions as a

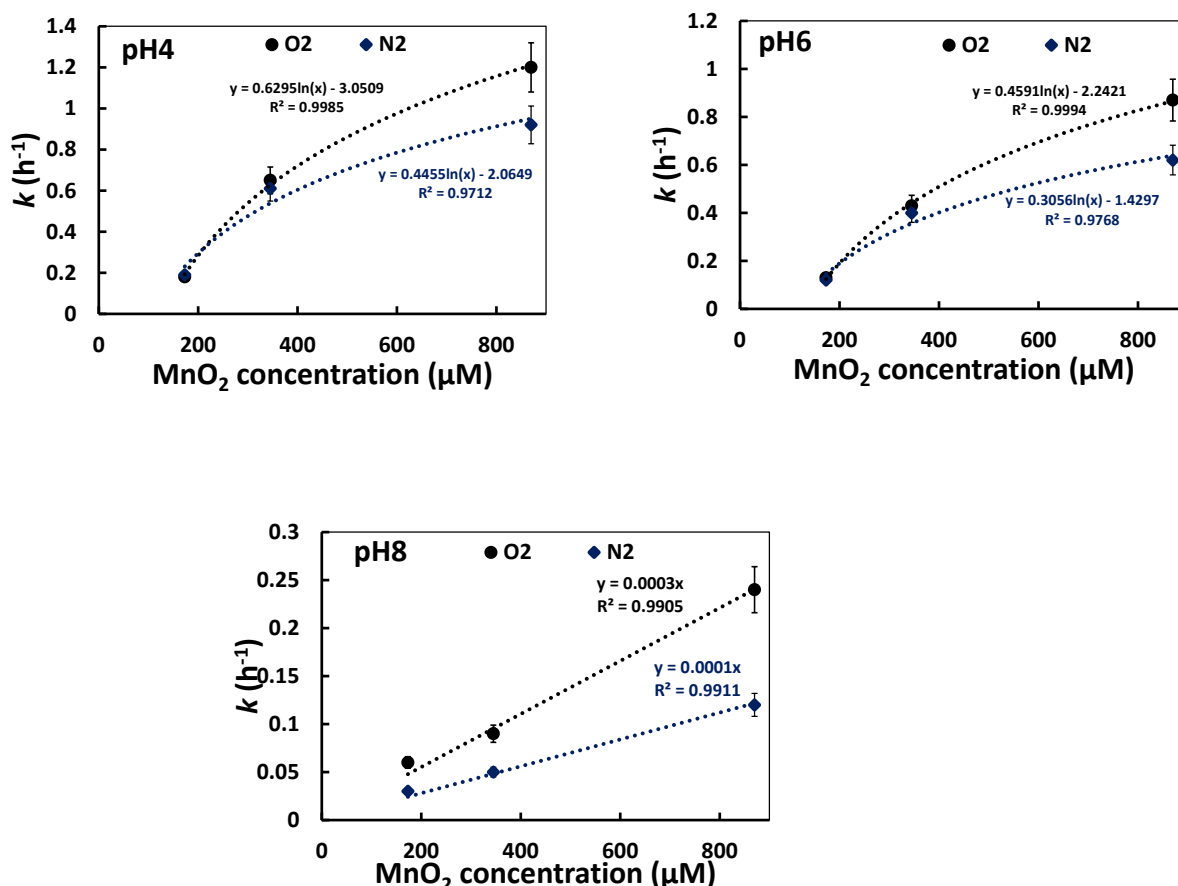
178 function of MnO<sub>2</sub> concentration (173-870 μM or 15 -75.6 mg/L) at three pH values (4.0,  
179 6.0, 8.0 (± 0.1)) over 8 hours of reaction time (Figure S4). The entire kinetic curve could  
180 not be properly described by simple equations that include classical exponential  
181 functions (*e.g.*, first- or second- order model), probably due to the complexity of  
182 involved reactions including accumulation and competition of reaction products (*e.g.*  
183 OFL byproducts, Mn(II) ions, etc.) and/or a gradual change of the reactivity of surface  
184 sites. For the sake of simplicity and to overcome possible interference caused by the  
185 accumulated byproducts, we have determined the rate constant over the first stage of  
186 reaction (*i.e.*, 1h). The initial rate constants  $k$  (h<sup>-1</sup>) calculated by linear regression of ln  
187 [OFL]/[OFL]<sub>0</sub> versus time, were plotted against MnO<sub>2</sub> concentration in Figure 1. The  
188 correlation coefficients (R<sup>2</sup>) of linear regression ( $\ln C/C_0 = -kt$ ) were more than 0.90  
189 for all experiments.

190 The rate constants exhibited the same order, pH 4.0 > pH 6.0 > pH 8.0, regardless of  
191 MnO<sub>2</sub> concentration. This is consistent with previous reports (Li et al., 2020; Zhang  
192 and Huang, 2005; Zhang et al., 2008), which showed that acidic conditions enabled  
193 higher quinolones removal in the presence of MnO<sub>2</sub>. This can be ascribed to more  
194 favorable interactions between the less negatively charged surface (pH<sub>IEP</sub> of MnO<sub>2</sub> ~  
195 2.0) and OFL (pK<sub>a</sub> 6.08 and 8.25, Figure S5) at acidic pH values. Furthermore, the  
196 decrease in redox potential of MnO<sub>2</sub> from 0.99 V to 0.76 V when the pH increased from  
197 4.0 to 8.0 would also explain the enhanced reactivity under acidic conditions, as  
198 previously reported (Li et al., 2020).

199 Mass balance showed that adsorption and oxidation are involved in the removal of OFL

200 in the presence of MnO<sub>2</sub>, even though the adsorption appears to be relatively weak for  
201 our experimental conditions (*e.g.*, less than 1.5 μmol m<sup>-2</sup>, at pH 6.0; less than 0.1 μmol  
202 m<sup>-2</sup>, at pH 8.0). Based on previous investigations for fluoroquinolones (Kamagate et al.,  
203 2019; Martin et al., 2015; Zhou et al., 2019), OFL may form metal-bonded complexes  
204 with surface sites and/or directly hydrogen-bonded complexes with surface hydroxo  
205 groups involving both carboxylate and keto groups. However, accurate quantification  
206 of the adsorption is not straightforward, because binding of redox-active compounds to  
207 birnessite is followed by an electron transfer process resulting in the concomitant  
208 oxidation of sorbed compound and reduction of surface-bound metal. LC/MS analysis  
209 showed that OFL oxidation passes through partial or full N-dealkylation of the  
210 piperazine ring, as two predominant products of *m/z* = 336 (M-26) and *m/z* = 279 (M-  
211 69) have been detected (See Figure S6 for more details). Indeed, the piperazine ring of  
212 OFL can be oxidized through two one-electron transfers from the N atom of piperazine  
213 ring to Mn(IV), and then N-dealkylation and/or C-hydroxylation causes ring opening,  
214 as typically observed for similar compounds (Zhang and Huang, 2005). Additionally,  
215 trace amounts of M+16, M-44 (decarboxylation), M-101 and M+30 were detected, as  
216 previously reported for the Mn-based oxidation of OFL (Li et al., 2021; Zhang and  
217 Huang, 2005).

218



219

220

221

222

223 **Figure 1.** Initial removal rate constants of OFL *versus* MnO<sub>2</sub> concentration at three pH values 4.0,  
 224 6.0, 8.0 (± 0.1). 173, 345, 870 μM (15, 30, 75.6 mg/L) MnO<sub>2</sub>; 10 μM OFL; 10 mM NaCl; under  
 225 anoxic (N<sub>2</sub>) and oxic (O<sub>2</sub>) conditions. Dashed lines are the best correlation obtained between *k* and  
 226 MnO<sub>2</sub> amount. Correlation coefficients (R<sup>2</sup>) are indicators of the strength of the linear or non-linear  
 227 relationship.

228

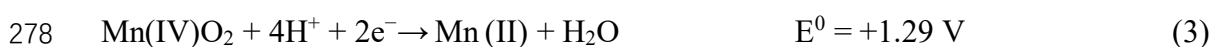
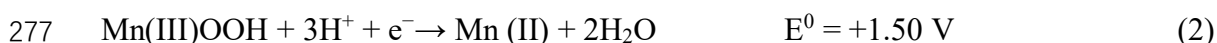
229 The effect of oxygen on the removal efficiency of OFL was only observed at high MnO<sub>2</sub>  
 230 concentration (870 μM) or at pH 8.0 ± 0.1 for the full range of MnO<sub>2</sub> concentration  
 231 (Figure 1). In both conditions, the apparent pseudo-first-order rate constant *k* (h<sup>-1</sup>)  
 232 increased with increasing MnO<sub>2</sub> concentration. It is worth noting that a linear  
 233 dependence of reactivity on MnO<sub>2</sub> amount was only observed at pH 8.0, while a  
 234 logarithmic relationship was observed at pH 4.0 and 6.0 (Figure 1). Contribution of  
 235 Fenton-like reaction through, for instance hydroxyl radical formation, in OFL removal

236 is excluded, since the addition of ethanol, used as a hydroxyl radical scavenger, has no  
237 effect on the OFL removal (Figure S7). Furthermore, we found that the impact of  
238 oxygen on birnessite reactivity at pH 8.0 is not specific to OFL, since similar behavior  
239 has been observed with another antibiotic compound, pipemidic acid (see Figure S8).  
240 It is generally known that the reaction of MnO<sub>2</sub> with redox-active compounds is  
241 complex and involves several reaction pathways that occur simultaneously. The redox  
242 byproducts generated through reductive dissolution of MnO<sub>2</sub> or OFL oxidation, can  
243 bind onto the MnO<sub>2</sub> surfaces, and alter the initial surface reactivity (*i.e.*, passivation).  
244 Generally, the generated Mn(II) is sorbed onto the MnO<sub>2</sub> surface and then oxidized.  
245 Mn(IV) is reduced, and the resulting product is Mn(III), which is commonly called the  
246 comproportionation reaction (Wang et al., 2019; Zhao et al., 2016). In addition, the  
247 adsorbed Mn(II) on vacant sites can be oxidized by O<sub>2</sub> at high pH to yield Mn(III).  
248 Because higher MnO<sub>2</sub> concentration enables more OFL oxidation (higher *k*, Figure 1),  
249 more reductive dissolution or Mn(II) production is expected. Dissolved Mn(II) was  
250 below the detection limit (< 0.02 μM for AAS) in all investigated conditions,  
251 confirming that generated Mn(II) by reductive dissolution of MnO<sub>2</sub> was completely  
252 removed by binding to MnO<sub>2</sub>. Competitive binding between OFL and Mn(II) at MnO<sub>2</sub>  
253 edge sites, and/or adsorption of OFL oxidation byproducts at the MnO<sub>2</sub> surface may  
254 also explain the passivation of the Mn-oxide surface. All these reactions are pH-  
255 dependent, as well as the passivation of MnO<sub>2</sub> surfaces. This may explain why the  
256 relationship between the oxidation rate constant of OFL and MnO<sub>2</sub> content is not linear  
257 over the whole pH range investigated (Figure 1). Furthermore, higher surface-oxidation

258 rates of Mn(II) at alkaline pH values (Lefkowitz et al., 2013; Namgung et al., 2014)  
259 may explain the pronounced impact of oxygen on birnessite reactivity at pH 8.0 (Figure  
260 1).

261 Collectively, these results suggest that enhanced removal efficiency of OFL under oxic  
262 conditions at high MnO<sub>2</sub> concentration or high pH is due to the Mn(III) generated  
263 through Mn(II) surface-catalyzed oxidation by oxygen. This is, however, in  
264 disagreement with a recent work which reported that oxygen inhibited phenol  
265 degradation by δ-MnO<sub>2</sub> because the generated Mn(III)-phases at the MnO<sub>2</sub> surface may  
266 block reactive sites and cause particle aggregation, thereby lowering the surface  
267 reactivity (Hu et al., 2019). This discrepancy with the present work may be explained  
268 by the difference in experimental conditions including target contaminant  
269 characteristics and its affinity to MnO<sub>2</sub> surfaces, and target compound/MnO<sub>2</sub> molar  
270 ratio.

271 On the other hand, previous works have reported that the Mn(III) oxides or Mn(III)  
272 complexes can rapidly oxidize a variety of organic compounds (Chen et al., 2013;  
273 Huang et al., 2018; Klewicki and Morgan, 1999; Nico and Zamoski, 2001). Mn(III) is a  
274 strong oxidant for one electron transfer reaction (Hu et al., 2017; Sun et al., 2021),  
275 compared to two electron transfer reaction involving Mn(IV).



279

280 In a heterogeneous system, the greater reactivity of Mn(III)-bearing phases has been  
281 explained by longer and weaker Mn(III)-O bonds facilitating the electron transfer with  
282 sorbing compounds (*e.g.*, phenol) (Huang et al., 2018; Ukrainczyk and McBride, 1992).  
283 It seems that direct coordination of Mn(III) with target compounds ensures to facilitate  
284 electron transfer without change in the Mn spin state, while the outer sphere electron  
285 transfer in surface Mn(IV) requires a change in the Mn spin state, in turn making the  
286 electron transfer process more difficult (Huang et al., 2018; Ukrainczyk and McBride,  
287 1992). Indeed, Mn(III) was reported to be as a high spin  $d^4$  ion with much lower ligand  
288 field stabilization energy and faster ligand exchange rates comparing with Mn(IV)  
289 (Nico and Zasoski, 2000). In contrast, other reports showed that Mn(III) sites are less  
290 reactive with respect to target contaminants. For example, lower As(III) oxidation have  
291 been attributed to the lower affinity of Mn(III) sites for As(III) adsorption, and slower  
292 electron transfer rates with adsorbed As(III) (Lafferty et al., 2010a; Lafferty et al.,  
293 2010b; Zhu et al., 2009). Moreover, the surface functional groups on Mn(III) sites are  
294 more labile than functional groups on Mn(IV) sites (Zhu et al., 2009), and therefore  
295 strong adsorption via ligand exchange processes on Mn(III) sites than on Mn(IV) sites  
296 is expected. Finally, different types of Mn sites, *e.g.*, Mn(III, IV) in sheets, Mn(III, IV)  
297 at edges, and Mn(III) in interlayers, likely have varying reactivity (Manceau et al., 1997;  
298 Simanova and Peña, 2015; Yu et al., 2012). The interlayer Mn(III) was suggested to be  
299 the dominant oxidizing site, and the abundance of Mn(III) with respect to total Mn may  
300 be key in promoting the reactivity of birnessite (Peng et al., 2017). From a kinetic point  
301 of view, Mn(III) at the edges seems to contribute at short reaction times, while Mn(III,  
302 IV) in the MnO<sub>2</sub> sheets is important at longer times (Simanova and Peña, 2015; Wang  
303 et al., 2018b). Despite this conflicting information about the role of structural Mn(III)  
304 in promoting MnO<sub>2</sub> reactivity, we may conclude that multiple factors may control the



305 contribution of Mn(III) in enhancing the removal capacity of birnessite. This may  
306 include the ratio of Mn(III) to Mn(IV), mineral phase transformation along the redox  
307 reaction, and properties of target contaminants and its interaction with Mn sites. To gain  
308 more insights into the underlying passivation mechanisms, the effects of Mn(II)/MnO<sub>2</sub>  
309 ratio on the removal kinetics of OFL were investigated under oxic and anoxic  
310 conditions in the following section.

311

### 312 **3.2. Combined effects of Mn(II) and O<sub>2</sub> under a wide range of ionic strength**

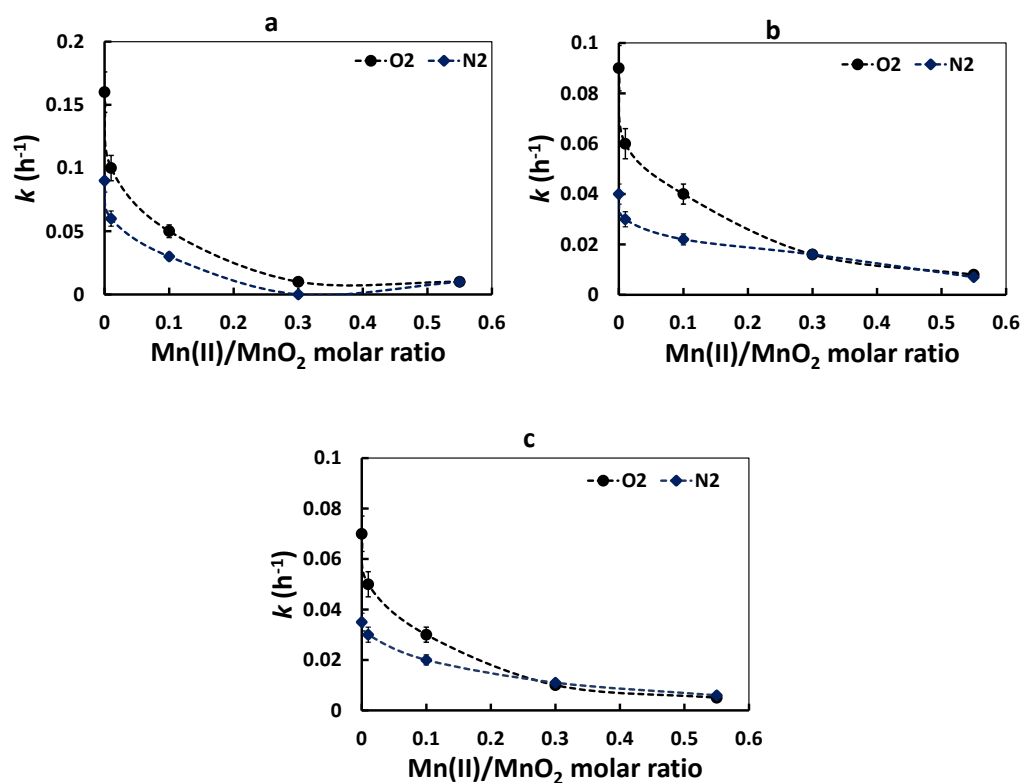
313 As an attempt to confirm the impact of surface-catalyzed oxidation of Mn(II) by O<sub>2</sub> on  
314 the reactivity of MnO<sub>2</sub>, OFL removal kinetics were investigated with different  
315 Mn(II)/MnO<sub>2</sub> molar ratios at pH 8.0 (Figure 2). As expected, the initial rate constants  
316 of OFL sharply decreased with increasing Mn(II) under both investigated conditions.  
317 As previously reported (Chen et al., 2010; Li et al., 2020; Remucal and Ginder-Vogel,  
318 2014), dissolved Mn(II) strongly adsorbed on the negatively charged birnessite surfaces,  
319 resulting in competition between OFL and Mn(II) binding to the reactive surface sites  
320 of MnO<sub>2</sub>. This Mn(II) binding is much more important at alkaline pH values (Lefkowitz  
321 et al., 2013). The adsorbed Mn(II) on vacant sites at high pH is oxidized to Mn(III)  
322 through surface-catalyzed oxidation of Mn(II) enabling more Mn(III) in the vacancies  
323 (Zhu et al., 2010). This explains why the dissolved Mn(II) concentration was found  
324 here below the AAS detection limit, even for the highest Mn(II) amount (200 μM).  
325 Time-dependent UV-Vis measurements for birnessite suspensions containing 200 μM  
326 Mn(II), suggested more generated Mn(III) in the presence of oxygen relative to anoxic  
327 conditions (Figure S9). Indeed, the intensity of adsorption bands at 258 nm for the  
328 potential Mn(III)-PP complex ( $\lambda_1 = 480 \text{ nm}$ ,  $\epsilon_1 = 65 \text{ M}^{-1}$ ;  $\lambda_2 = 258 \text{ nm}$ ,  $\epsilon_2 = 6750 \text{ M}^{-1}$ )  
329 (Hu et al., 2017) was found to be higher under oxic conditions.

330 It should be noted that the greater reactivity of birnessite under oxic conditions relative  
331 to anoxic systems is only observed at lower Mn(II)/MnO<sub>2</sub> molar ratio ( $\leq 0.1$ ). At higher  
332 ratio, strong competition between Mn(II) and OFL may act as a counterweight to the  
333 Mn(III) contribution, thereby reducing the overall reactivity of MnO<sub>2</sub>.

334

335 When removal kinetics was investigated at higher ionic strength (10 or 100 mM of  
336 NaCl), a decrease in the initial rate constants of OFL was observed, mainly under oxic  
337 conditions and at low Mn(II)/MnO<sub>2</sub> molar ratio (Figure 2). Increasing ionic strength  
338 may increase the size of MnO<sub>2</sub> via oriented aggregations (Burrows et al., 2012; Yang  
339 et al., 2019), thereby reducing the surface reactivity. This decrease in surface reactivity  
340 has also been previously observed during aging of manganese oxides through  
341 coalescence of particles (Stone and Morgan, 1984). Furthermore, Na<sup>+</sup> ions may  
342 compete with the cationic Mn(II) and/or zwitterionic form of OFL ( $pK_{a,1} = 6.08$  and  
343  $pK_{a,2} = 8.25$ ) for negatively charged adsorptive sites on MnO<sub>2</sub> ( $pH_{IEP} \sim 2.0$ ). Na<sup>+</sup> can  
344 occupy the interlayers of birnessite, potentially competing with Mn(II) and/or  
345 influencing the diffusion process of Mn(II) at reactive surface sites (Yang et al., 2019).  
346 Previous work reported similar competitive binding due to the presence of monovalent  
347 or divalent cations, resulting in decrease in the rate and magnitude of organic compound  
348 transformation (Chen et al., 2010). Under oxic conditions, oxidation of Mn(II) into  
349 Mn(III) and subsequent incorporation of Mn(III) into the layers may occur, resulting in  
350 birnessite transformation from hexagonal to orthogonal layer symmetry (Zhao et al.,  
351 2016). In this case, Na<sup>+</sup> ions could compensate for the charge deficiency caused by the  
352 presence of Mn(III), and subsequently act to stabilize Mn(III) in the layers (Drits et al.,  
353 2007; Zhu et al., 2010). This may explain the pronounced effect of increasing NaCl  
354 concentration on the MnO<sub>2</sub> surface reactivity in the presence of O<sub>2</sub>.

355



356

357

358

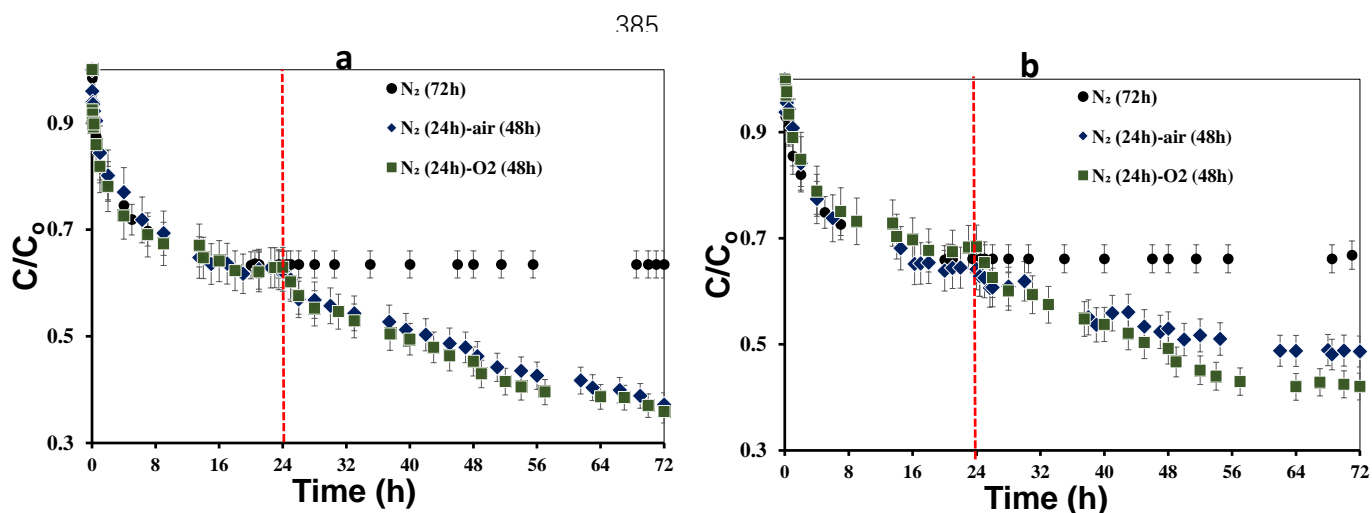
359

360 **Figure 2.** Initial removal rate constants of OFL as a function of Mn(II)/MnO<sub>2</sub> molar ratio under  
361 anoxic or oxic conditions. pH 8.0 ( $\pm$  0.1), 345  $\mu$ M (30 mg/L) acid birnessite. 0, 5, 50, 100, 200  $\mu$ M  
362 Mn(II); 10  $\mu$ M OFL; (a) 0 mM NaCl, (b) 10 mM NaCl, (c) 100 mM NaCl. Dashed lines are only as  
363 visual guide.

364

365 To check whether transition zones at oxic-anoxic interfaces may influence the reactivity  
366 of birnessite, removal kinetics experiments were conducted for 24 h under N<sub>2</sub>, with  
367 subsequent ambient air conditions or bubbling O<sub>2</sub> for 48h (Figure 3). Under anoxic  
368 conditions, a plateau was observed at around 16h, and then continued over 72 h. When  
369 suspensions were exposed to ambient air or O<sub>2</sub> after a pre-equilibration period of 24h  
370 under N<sub>2</sub>, OFL was further removed up to 65% in suspension, which could be ascribed  
371 to the Mn(III) generated through Mn(II) surface-catalyzed oxidation by oxygen. As  
372 mentioned above, these newly generated Mn(III) are more reactive for OFL oxidation.  
373 It should be noted that strong oxygenation of solution with bubbling O<sub>2</sub> has no greater  
374 effect on the birnessite reactivity, as compared to the solution exposed to ambient air.

375 The same two-step anoxic/oxic process was repeated but in the presence of 5  $\mu\text{M}$  Mn(II).  
 376 This Mn(II) amount was chosen to cover the typical range of Mn concentration found  
 377 in surface and groundwaters ( $\sim 4 \mu\text{M}$ ) (Namgung et al., 2014). The presence of 5  $\mu\text{M}$   
 378 Mn(II) did not significantly affect the removal rate whether under oxic or anoxic  
 379 conditions. Only a slight inhibition was observed especially for longer reaction times ,  
 380 likely because of competitive effects of Mn(II) and OFL for binding onto reactive sites.  
 381 In all conditions, removal kinetic exhibited a plateau under  $\text{N}_2$ , followed by a drop in  
 382 the aqueous concentration of OFL when the reaction media was exposed to air or  $\text{O}_2$   
 383 (Figure 3).  
 384



386 **Figure 3.** Removal kinetics of OFL in dynamic same two-step anoxic/oxic process: (a) 0  $\mu\text{M}$  Mn(II);  
 387 (b) 5  $\mu\text{M}$  Mn(II). pH 8.0 ( $\pm 0.1$ ); 10  $\mu\text{M}$  OFL; 10 mM NaCl; 345  $\mu\text{M}$  acid birnessite. The red vertical  
 388 line indicates the beginning of oxygenation through exposure to ambient air or with bubbling  $\text{O}_2$ .  
 389

### 390 3.3. XRD and XPS investigations

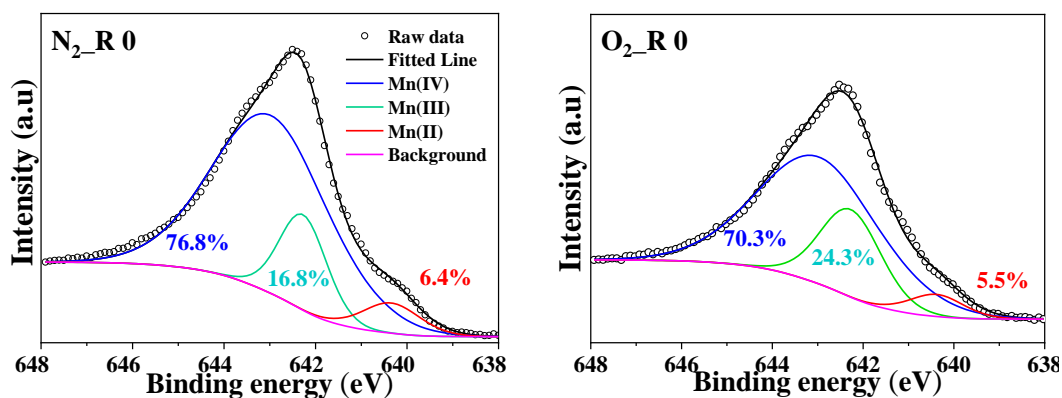
391 To evaluate the role of Mn speciation on reactivity changes and the passivation of the  
 392  $\text{MnO}_2$  surface, XPS analysis of initial and reacted  $\text{MnO}_2$  samples were performed under  
 393 defined experimental conditions.

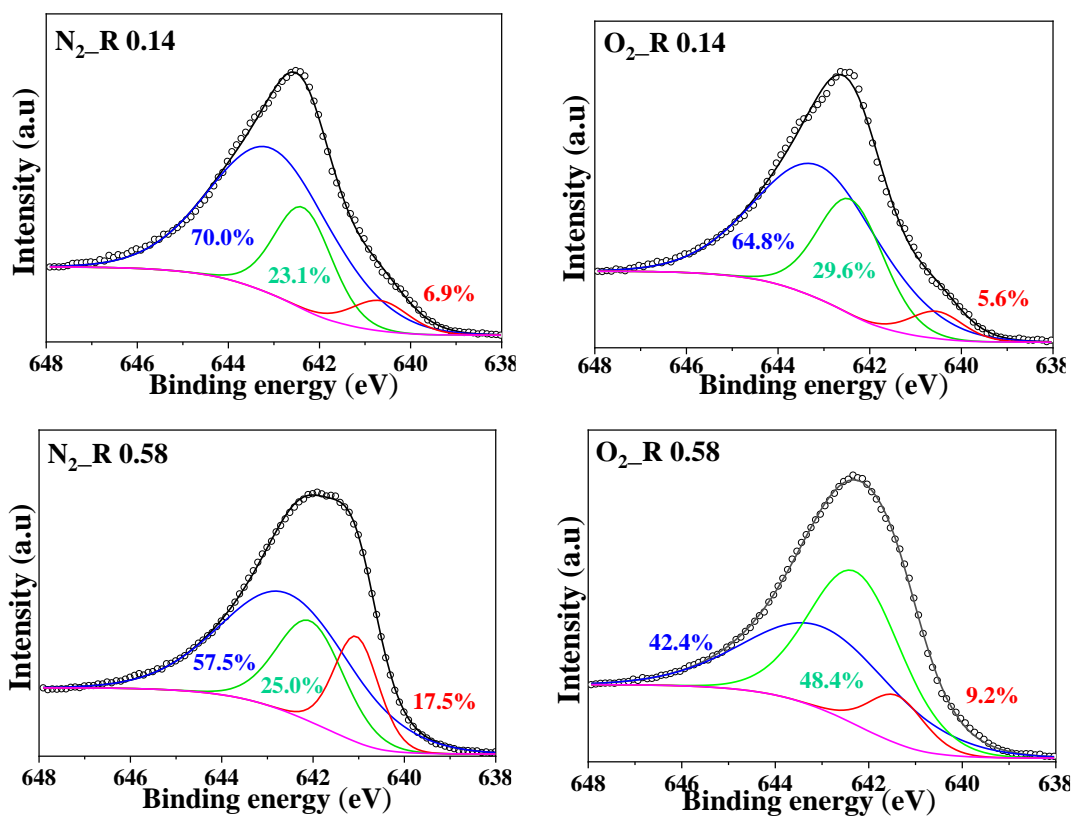
394 First, the total contents of major elements are reported in Table S1. In the absence of  
 395 Mn(II), a decrease in Mn content in reacted samples was observed, likely resulting from

396 the presence of various adsorbing ligands at the surface (Table S1) (Shaikh et al., 2016).  
397 Higher Na content under oxic conditions also proved the compensation effect of Na<sup>+</sup> as  
398 discussed above. Increasing Mn(II) concentrations from 50 μM to 200 μM enhanced  
399 Mn percentage, likely because of the adsorption of Mn(II) onto the MnO<sub>2</sub> surfaces. K  
400 content was below detection limit, likely due to the large adsorption amounts of Mn  
401 exchanging with interlayer K<sup>+</sup> ion.

402 Second, the high resolution spectra of Mn 2p<sub>3/2</sub> was then fitted and the BE (binding  
403 energy) positions of Mn(II), Mn(III), Mn(IV) ranged from 640.1 to 641.4 eV, from  
404 642.1 to 642.4 eV and from 642.6 to 643.1 eV respectively, consistent with previously  
405 reported values (Figure 4, Table S2) (Sun et al., 2019; Tang et al., 2013; Tang et al.,  
406 2014). We have subsequently determined the average oxidation state (AOS) of all  
407 samples, and found that the AOS (initial value 3.87) decreased for all reacted samples  
408 (Table S2).

409 As expected, increasing the Mn(II) concentration from 0 μM to 200 μM enhanced the  
410 amount of Mn(II) bond to MnO<sub>2</sub> surfaces (Figure 4). An increase in the percentage of  
411 Mn(III) was also observed in the presence of oxygen relative to anoxic conditions,  
412 while that of Mn(IV) decreased. As previously explained, Mn(II) can undergo surface-  
413 catalyzed oxidation by molecular oxygen and/or comproportionation with structural  
414 Mn(IV) forming Mn(III) sites. Both processes can enhance the Mn(III) content in MnO<sub>2</sub>,  
415 particularly under oxic conditions (Table S2).





417

418

419

420 **Figure 4.** Fitting of Mn  $2p_{3/2}$  XPS high resolution spectra of the synthesized pristine acid birnessite  
 421 and samples treated with Mn(II) and OFL under anoxic and oxic conditions. The R represents the  
 422 Mn(II)/MnO<sub>2</sub> molar ratio. 345  $\mu$ M acid birnessite; 10  $\mu$ M OFL; 10 mM NaCl; 0, 50, 200  $\mu$ M Mn(II);  
 423 48 h reaction time; pH 8.0 ( $\pm$ 0.1). The numbers inset are the percentage of Mn(II) (red), Mn(III)  
 424 (green) and Mn(IV) (blue).

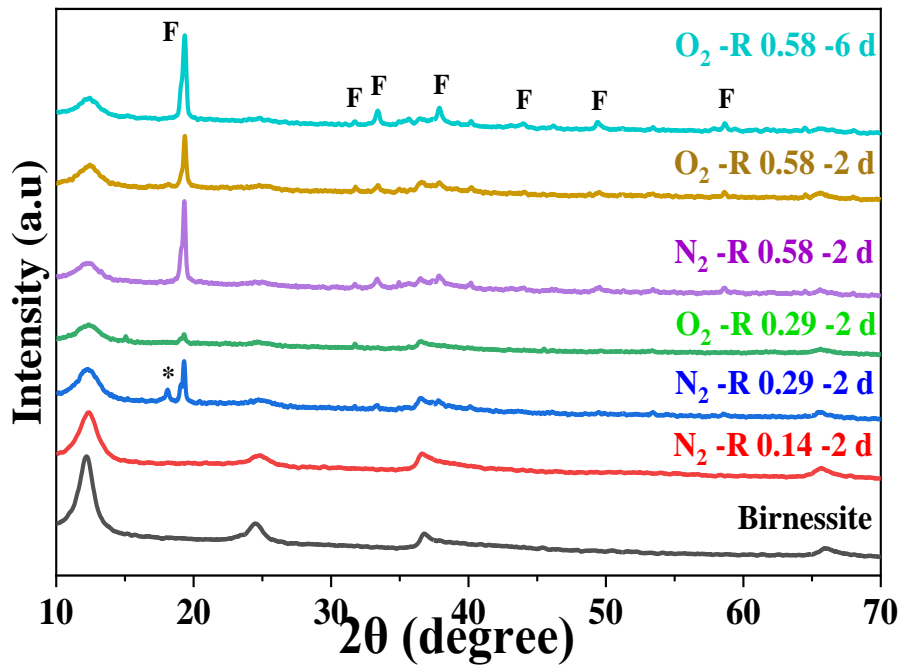
425

426 The high-resolution spectra of O1s were then evaluated to assess potential  
 427 transformation of birnessite surfaces (Table S3 and Figure S10). The compositions of  
 428 oxygen bonding types consisted of a main peak located at around 530.2 eV  
 429 corresponding to lattice oxygen with metal ( $O_{\text{latt}}$ ), a shoulder peak near 531.6 eV  
 430 attributing to the adsorbed oxygen species on MnO<sub>2</sub> surface ( $O_{\text{ads}}$ ) in the form of  
 431 hydroxide oxygen ( $\text{OH}^-$ ) and the weakest peak at higher binding energy assigning to  
 432 the adsorbed oxygen in water molecule ( $O_{\text{surf}}$ ) (Tang et al., 2013; Zhang et al., 2020).  
 433 After reaction, the increased proportions of H<sub>2</sub>O suggested that the surface became  
 434 progressively hydroxylated and hydrated. It is worth noting that in the presence of  
 435 200  $\mu$ M Mn(II), high contents in Mn(III) and  $\text{OH}^-$  under anoxic condition have been

436 considered as characteristic of intermediate reaction products Mn(III)-hydroxide, here  
437 represented as MnOOH (Nesbitt et al., 1998). Moreover, the content of  $O_{\text{latt}}$  decreased  
438 to 49 % (anoxic) and 65 % (oxic), which suggests that lattice oxygen may participate  
439 in the oxidation of Mn(II) with the formation of oxygen vacancy (Cheng et al., 2019).  
440 Once the  $O_{\text{latt}}$  is consumed, dissolved oxygen could compensate (Cheng et al., 2019),  
441 which would explain the difference in  $O_{\text{latt}}$  content between anoxic and oxic  
442 environments.

443 The produced Mn(III) may incorporate into the layer of birnessite and induce the  
444 changes of mineral structure by converting birnessite into lower valence Mn phases  
445 (Zhao et al., 2016). To check possible phase transformation, XRD analysis of  $\text{MnO}_2$   
446 samples under various Mn(II)/ $\text{MnO}_2$  molar ratios (R) and under anoxic and oxic  
447 conditions was conducted (Figure 5). Samples reacted with OFL in the presence of  
448 dissolved Mn(II) (50  $\mu\text{M}$ , R = 0.14) showed no bulk transformation. However, XRD  
449 data of samples with higher R (i.e. 0.29 or 0.58) showed different peaks, both under  
450 anoxic and oxic conditions, which could suggest the presence of lower valence Mn  
451 oxides, e.g. feitknechte ( $\beta\text{-MnOOH}$ ) (Wang et al., 2018a; Lefkowitz et al., 2013). This  
452 is consistent with SEM images where needle-shaped particles were observed amid  
453 nanoflower-shaped particles of birnessite, especially at higher Mn(II) concentration and  
454 under oxic conditions (Figure S11). These needle-shaped crystals can be attributed  
455 either to the presence of manganite ( $\gamma\text{-MnOOH}$ ) as previously reported by *e.g.* Larsen  
456 et al., (1998), or more certainly according to XRD data, to feitknechte as previously  
457 reported by Lefkowitz et al., (2013).

458



459

460 **Figure 5.** XRD patterns of the MnO<sub>2</sub> samples treated with Mn(II) and OFL under oxic and anoxic  
 461 conditions. 345 μM acid birnessite; 10 μM OFL; 10 mM NaCl; 0, 50, 100, 200 μM Mn(II); 48 h or  
 462 6 d reaction time; pH 8.0 (± 0.1). The R represents the Mn(II)/MnO<sub>2</sub> molar ratio. The **f** symbols  
 463 indicate XRD peaks visible on the feitknechtite (β-MnOOH) sample in Lefkowitz et al., 2013; the  
 464 \* symbol has previously been attributed to hausmannite (Wang et al., 2018a) but in the absence of  
 465 the main Bragg peaks of this phase, it would rather belong to an hydrated α-MnO<sub>2</sub> phase (Rossouw  
 466 et al., 1992).

467

## 468 **Conclusions**

469 As a result of natural or anthropogenic activities, such as groundwater recharge,  
 470 sediment dredging, water table fluctuations, etc., alternating redox conditions  
 471 commonly occur in natural systems. Here, we have demonstrated for the first time that  
 472 the oxygen can alter the redox reactivity of MnO<sub>2</sub> under environmentally-relevant  
 473 conditions of Mn(II) dosage, pH and ionic strength. A decline in the oxidation rate  
 474 constant with increasing pH was observed, likely because of the decrease in the redox  
 475 potential of MnO<sub>2</sub> at higher pH and modification in surface interactions with the target  
 476 compound. At high pH, the adsorbed Mn(II) on vacant sites can be oxidized by O<sub>2</sub> or  
 477 Mn(IV) surrounding the vacant sites into Mn(III) (comproportionation reaction).



478 Therefore, OFL adsorbed at vacant sites can be oxidized by the newly generated Mn(III)  
479 sites, which seems to be strong oxidizing species. However, excess dissolved Mn(II)  
480 would compete with compounds for binding at reactive sites, thus decreasing the  
481 removal capacity of birnessite. The decreased reactivity of MnO<sub>2</sub> with higher ionic  
482 strength also suggested that the sorption of alkali cation (Na<sup>+</sup>) on the surface may  
483 control the birnessite reactivity. Furthermore, sequential anoxic-oxic dynamic process  
484 may significantly impact the fate of existing contaminants in the presence of birnessite.  
485 Combining anoxic and oxic environments into one process may be relevant in many  
486 subsurface environments, for instance, when anoxic aquifers and/or sediments come  
487 into contact with oxygen. Further redox oscillation studies are needed to explore the  
488 fate and mobility of contaminants and co-existing natural compounds (*e.g.*, dissolved  
489 organic matter), in the presence of manganese oxides.

490

#### 491 **Acknowledgments**

492 Q.L thanks the Chinese Scholarship Council of PR China for her Ph.D. grant and  
493 Rennes Métropole (France) for a mobility grant for an extended research visit at KIT  
494 (Germany). We want to acknowledge Valerie Courousse (AAS) and Kouhail Yasmine  
495 (XRD) for providing help in experiments.

496

497 **References**

- 498 Burrows, N.D., Hale, C.R.H., Penn, R.L., 2012. Effect of ionic strength on the kinetics of crystal growth  
499 by oriented aggregation. *Cryst. Growth. Des.* 12, 4787-4797.
- 500 Chen, W., Ding, Y., Johnston, C.T., Teppen, B.J., Boyd, S.A., Li, H., 2010. Reaction of lincosamide  
501 antibiotics with manganese oxide in aqueous solution. *Environ. Sci. Technol.* 44, 4486-4492.
- 502 Chen, W.R., Liu, C., Boyd, S.A., Teppen, B.J., Li, H., 2013. Reduction of carbadox mediated by reaction  
503 of Mn(III) with oxalic acid. *Environ. Sci. Technol.* 47, 1357-1364.
- 504 Cheng, Y., Huang, T., Liu, C., Zhang, S., 2019. Effects of dissolved oxygen on the start-up of manganese  
505 oxides filter for catalytic oxidative removal of manganese from groundwater. *Chem. Eng. J.* 371,  
506 88-95.
- 507 Davies, S.H.R., James J, M., 1989. Manganese(II) Oxidation Kinetics on Metal Oxide Surfaces. *J.*  
508 *Colloid Interface Sci.* 129, 63-77.
- 509 Diem, D., Stumm, W., 1984. Is dissolved  $Mn^{2+}$  being oxidized by  $O_2$  in absence of Mn-bacteria or surface  
510 catalysts? *Geochim. Cosmochim. Acta.* 48, 1571-1573.
- 511 Drits, V.A., Lanson, B., Gaillot, A., 2007. Birnessite polytype systematics and identification by powder  
512 X-ray diffraction. *Am. Mineral.* 92, 771-788.
- 513 Elzinga, E.J., 2011. Reductive Transformation of Birnessite by Aqueous Mn(II). *Environ. Sci. Technol.*  
514 45, 6366-6372.
- 515 Elzinga, E.J., 2016.  $^{54}Mn$  radiotracers demonstrate continuous dissolution and reprecipitation of  
516 vernadite ( $\delta$ - $MnO_2$ ) during interaction with aqueous Mn (II). *Environ. Sci. Technol.* 50, 8670-8677.
- 517 Hinkle, M.A.G., Orcid, K.G.D., Catalano, J.G., 2017. Impact of Mn(II)-Manganese Oxide Reactions on  
518 Ni and Zn Speciation. *Environ. Sci. Technol.* 51, 3187-3196.
- 519 Hu, E., Zhang, Y., Wu, S., Wu, J., Liang, L., He, F., 2017. Role of dissolved Mn(III) in transformation  
520 of organic contaminants: Non-oxidative versus oxidative mechanisms. *Water. Res.* 111, 234-243.
- 521 Hu, E., Pan, S., Zhang, W., Zhao, X., Liao, B., He, F., 2019. Impact of dissolved  $O_2$  on phenol oxidation  
522 by  $\delta$ - $MnO_2$ . *Environ. Sci. Processes Impacts.* 21, 2118-2127.
- 523 Huang, J., Zhong, S., Dai, Y., Liu, C., Zhang, H., 2018. Effect of  $MnO_2$  Phase Structure on the Oxidative  
524 Reactivity toward Bisphenol A Degradation. *Environ. Sci. Technol.* 52, 11309-11318.
- 525 Jeong, H.Y., Han, Y., Park, S.W., Hayes, K.F., 2010. Aerobic oxidation of mackinawite (FeS) and its  
526 environmental implication for arsenic mobilization. *Geochim. Cosmochim. Acta.* 74, 3182-3198.
- 527 Junta, J.L., Hochella, Jr, M.F., 1994. Manganese (II) oxidation at mineral surfaces: A microscopic and  
528 spectroscopic study. *Geochim. Cosmochim. Acta.* 58, 4985-4999.
- 529 Kamagate, M., Pasturel, M., Brigante, M., Hanna, K., 2019. Mineralization Enhancement of  
530 Pharmaceutical Contaminants by Radical-Based Oxidation Promoted by Oxide-Bound Metal Ions.  
531 *Environ. Sci. Technol.* 54, 476-485.
- 532 Klewicki, J., Morgan, J., 1999. Dissolution of  $\beta$ - $MnOOH$  particles by ligands: pyrophosphate,  
533 ethylenediaminetetraacetate, and citrate. *Geochim. Cosmochim. Acta.* 63, 3017-3024.
- 534 Lafferty, B.J., Ginder-Vogel, M., Sparks, D.L., 2010a. Arsenite Oxidation by a Poorly Crystalline  
535 Manganese-Oxide 1. Stirred-Flow Experiments. *Environ. Sci. Technol.* 44, 8460-8466.
- 536 Lafferty, B.J., Ginder-Vogel, M., Zhu, M., Livi, K.J.T., Sparks, D.L., 2010b. Arsenite Oxidation by a  
537 Poorly Crystalline Manganese-Oxide. 2. Results from X-ray Absorption Spectroscopy and X-ray  
538 Diffraction. *Environ. Sci. Technol.* 44, 8467-8472.

539 Lan, S., Wang, X., Xiang, Q., Yin, H., Tan, W., Qiu, G., Liu, F., Zhang, J., Feng, X., 2017. Mechanisms  
540 of Mn(II) catalytic oxidation on ferrihydrite surfaces and the formation of manganese  
541 (oxyhydr)oxides. *Geochim. Cosmochim. Acta.* 211, 79-96.

542 Larsen, I., Little, B., Nealson, K.H., Ray, R., Stone, A., Tian, J., 1998. Manganite reduction by  
543 *Shewanella putrefaciens* MR-4. *Am. Mineral.* 83, 1564-1572.

544 Lefkowitz, J.P., Elzinga, E.J., 2015. Impacts of Aqueous Mn(II) on the Sorption of Zn(II) by Hexagonal  
545 Birnessite. *Environ. Sci. Technol.* 49, 4886-4893.

546 Lefkowitz, J.P., Rouff, A.A., Elzinga, E.J., 2013. Influence of pH on the Reductive Transformation of  
547 Birnessite by Aqueous Mn(II). *Environ. Sci. Technol.* 47, 10364-10371.

548 Li, K., Xu, A., Wu, D., Zhao, S., Meng, T., Zhang, Y., 2021. Degradation of ofloxacin by a manganese-  
549 oxidizing bacterium *Pseudomonas* sp. F2 and its biogenic manganese oxides. *Bioresour. Technol.*  
550 328, 124826.

551 Li, Q., Pokharel, R., Zhou, L., Pasturel, M., Hanna, K., 2020. Coupled effects of Mn(II), pH and anionic  
552 ligands on the reactivity of nanostructured birnessite. *Environ. Sci. Nano.* 7, 4022-4031.

553 Luther, G.W., 2005. Manganese(II) Oxidation and Mn(IV) Reduction in the Environment—Two One-  
554 Electron Transfer Steps Versus a Single Two-Electron Step. *Geomicrobiol. J.* 22, 195-203.

555 Manceau, A., Silvester, E., Bartoli, C., Lanson, B., Drits, V.A., 1997. Structural mechanism of  $\text{Co}^{2+}$   
556 oxidation by the phyllo-manganate busserite. *Am. Mineral.* 82, 1150-1175.

557 Martin, S., Shchukarev, A., Hanna, K., Boily, J., 2015. Kinetics and mechanisms of ciprofloxacin  
558 oxidation on hematite surfaces. *Environ. Sci. Technol.* 49, 12197-12205.

559 McKenzie, R.M., 1971. The synthesis of birnessite, cryptomelane, and some other oxides and hydroxides  
560 of manganese. *Mineral. Mag.* 38, 493-502.

561 Namgung, S., Kwon, M.J., Qafoku, N.P., Lee, G., 2014.  $\text{Cr}(\text{OH})_3$  (s) Oxidation Induced by Surface  
562 Catalyzed Mn(II) Oxidation. *Environ. Sci. Technol.* 48, 10760-10768.

563 Namgung, S., Guo, B., Sasaki, K., Lee, S.S., Lee, G., 2020. Macroscopic and microscopic behaviors of  
564 Mn(II) (ad)sorption to goethite with the effects of dissolved carbonates under anoxic conditions.  
565 *Geochim. Cosmochim. Acta.* 277, 300-319.

566 Nesbitt, H.W., Canning, G.W., Bancroft, G.M., 1998. XPS study of reductive dissolution of  $7\text{\AA}$ -  
567 birnessite by  $\text{H}_3\text{AsO}_3$ , with constraints on reaction mechanism. *Geochim. Cosmochim. Acta.* 62,  
568 2097-2110.

569 Nico, P.S., Zasoski, R.J., 2000. Importance of Mn (III) availability on the rate of Cr(III) oxidation on  $\delta$ -  
570  $\text{MnO}_2$ . *Environ. Sci. Technol.* 34, 3363-3367.

571 Nico, P.S., Zasoski, R.J., 2001. Mn (III) center availability as a rate controlling factor in the oxidation of  
572 phenol and sulfide on  $\delta$ - $\text{MnO}_2$ . *Environ. Sci. Technol.* 35, 3338-3343.

573 Nico, P.S., Anastasio, C., Zasoski, R.J., 2002. Rapid photo-oxidation of Mn(II) mediated by humic  
574 substances. *Geochim. Cosmochim. Acta.* 66, 4047-4056.

575 Peng, H., McKendry, I.G., Ding, R., Thenuwara, A.C., Kang, Q., Shumlas, S.L., Strongin, D.R., Zdillab,  
576 M.J., Perdew, J.P., 2017. Redox properties of birnessite from a defect perspective. *Proc. Natl. Acad.*  
577 *Sci. U.S.A.* 114, 9523-9528.

578 Pokharel, R., Li, Q., Zhou, L., Hanna, K., 2020. Water Flow and Dissolved MnII Alter Transformation  
579 of Pipemidic Acid by Manganese Oxide. *Environ. Sci. Technol.* 54, 8051-8060.

580 Rossouw, M.H., Liles, D.C., Thackeray, M.M., David, W.I.F., Hull, S., 1992. Alpha manganese dioxide  
581 for lithium batteries: a structural and electrochemical study. *Mat. Res. Bull.* 27, 221-230.

582 Post, J.E., 1999. Manganese oxide minerals: crystal structures and economic and environmental  
583 significance. *Proc. Natl. Acad. Sci. U.S.A.* 96, 3447-3454.

584 Remucal, C.K., Ginder-Vogel, M., 2014. A critical review of the reactivity of manganese oxides with  
585 organic contaminants. *Environ. Sci. Processes Impacts*. 16, 1247-1266.

586 Seah, M.P., Gilmore, I.S., Beamson, G., 1998. XPS: Binding Energy Calibration of Electron  
587 Spectrometers 5ÈRe-evaluation of the Reference Energies. *Surf Interface Anal.* 26, 642-649.

588 Shaikh, N., Taujale, S., Zhang, H., Artyushkova, K., Ali, A.S. Cerrato J.M., 2016. Spectroscopic  
589 Investigation of Interfacial Interaction of Manganese Oxide with Triclosan, Aniline, and Phenol.  
590 *Environ. Sci. Technol.* 50, 10978-10987.

591 Simanova, A.A., Peña, J., 2015. Time-Resolved Investigation of Cobalt Oxidation by Mn(III)-Rich  $\delta$ -  
592  $MnO_2$  Using Quick X-ray Absorption Spectroscopy. *Environ. Sci. Technol.* 49, 10867-10876.

593 Stone, A.T., Morgan, J.J., 1984. Reduction and Dissolution of Manganese(III) and Manganese(IV)  
594 Oxides by organics. 1. Reaction with hydroquinone. *Environ. Sci. Technol.* 18, 450-456.

595 Sun, Q., Cui, P., Liu, C., Peng, S., Alves, M.E., Zhou, D., Shi, Z., Wang, Y., 2019. Antimony oxidation  
596 and sorption behavior on birnessites with different properties ( $\delta$ - $MnO_2$  and triclinic birnessite).  
597 *Environ. Pollut.* 246, 990-998.

598 Sun, Y., Im, J., Shobnam, N., Fanourakis, S.K., He, L., Anovitz, L.M., Erickson, P.R., Sun, H., Zhuang,  
599 J., Löffler, F.E., 2021. Degradation of Adsorbed Bisphenol A by Soluble Mn(III). *Environ. Sci.*  
600 *Technol.* 55, 13014-13023.

601 Tang, Q., Jiang, L., Liu, J., Wang, S., Sun, G., 2013. Effect of Surface Manganese Valence of Manganese  
602 Oxides on the Activity of the Oxygen Reduction Reaction in Alkaline Media. *ACS Catal.* 4, 457-  
603 463.

604 Tang, W., Wu, X., Li, D., Wang, Z., Liu, G., Liu, H., Chen, Y., 2014. Oxalate route for promoting activity  
605 of manganese oxide catalysts in total VOCs'oxidation: effect of calcination temperature and  
606 preparation method. *J. Mater. Chem. A*, 2, 2544-2554.

607 Ukrainczyk, L., McBride, M.B., 1992. Oxidation of Phenol in Acidic Aqueous Suspensions of  
608 Manganese Oxides. *Clays Clay Miner.* 40, 157-166.

609 Wang, Q., Yang, P., Zhu, M., 2018a. Structural Transformation of Birnessite by Fulvic Acid under  
610 Anoxic Conditions. *Environ. Sci. Technol.* 52, 1844-1853.

611 Wang, Q., Yang, P., Zhu, M., 2019. Effects of metal cations on coupled birnessite structural  
612 transformation and natural organic matter adsorption and oxidation. *Geochim. Cosmochim. Acta.*  
613 250, 292-310.

614 Wang, Y., Benkaddour, S., Marafatto, F.F., Peña, J., 2018b. Diffusion- and pH-Dependent Reactivity of  
615 Layer-Type  $MnO_2$ : Reactions at Particle Edges versus Vacancy Sites. *Environ. Sci. Technol.* 52,  
616 3476-3485.

617 Wilson, D.E., 1980. Surface and complexation effects on the rate of Mn(II) oxidation in natural waters.  
618 *Geochim. Cosmochim. Acta.* 44, 1311-1371.

619 Wu, J., Zhao, J., Hou, J., Xing, B., 2020. The Fate of p-Nitrophenol in Goethite-Rich and Sulfide-  
620 Containing Dynamic Anoxic/Oxic Environments. *Environ. Sci. Technol.* 54, 9427-9436.

621 Yang, P., Lee, S., Post, J.E., Xu, H., Wang, Q., Xu, W., Zhu, M., 2018. Trivalent manganese on vacancies  
622 triggers rapid transformation of layered to tunneled manganese oxides (TMOs): Implications for  
623 occurrence of TMOs in low-temperature environment. *Geochim. Cosmochim. Acta.* 240, 173-190.

624 Yang, P., Post, J.E., Wang, Q., Xu, W., Geiss, R., McCurdy, P.R., Zhu, M., 2019. Metal Adsorption  
625 Controls Stability of Layered Manganese Oxides. *Environ. Sci. Technol.* 53, 7453-7462.

626 Yu, Q., Sasaki, K., Tanaka, K., Ohnuki, T., Hirajima, T., 2012. Structural factors of biogenic birnessite  
627 produced by fungus *Paraconiothyrium* sp. WL-2 strain affecting sorption of  $\text{Co}^{2+}$ . *Chem. Geol.* 310-  
628 311, 106-113.

629 Zhang, H., Huang, C., 2005. Oxidative Transformation of Fluoroquinolone Antibacterial Agents and  
630 Structurally Related Amines by Manganese Oxide. *Environ. Sci. Technol.* 39, 4474-4483.

631 Zhang, H., Chen, W., Huang, C., 2008. Kinetic Modeling of Oxidation of Antibacterial Agents by  
632 Manganese Oxide. *Environ. Sci. Technol.* 42, 5548-5554.

633 Zhang, H., Xu, F., Xue, J., Chen, S., Wang, J., and Yang, Y., 2020. Enhanced removal of heavy metal  
634 ions from aqueous solution using manganese dioxide-loaded biochar: Behavior and mechanism.  
635 *Sci. Rep.* 10, 1-13.

636 Zhao, H., Zhu, M., Li, W., Elzinga, E.J., Villalobos, M., Liu, F., Zhang, J., Feng, X., Sparks, D.L., 2016.  
637 Redox Reactions between Mn(II) and Hexagonal Birnessite Change Its Layer Symmetry. *Environ.*  
638 *Sci. Technol.* 50, 1750-1758.

639 Zhao, J., Su, A., Tian, P., Tang, X., Collins, R.N., He, F., 2021. Arsenic (III) removal by  
640 mechanochemically sulfidated microscale zero valent iron under anoxic and oxic conditions. *Water*.  
641 *Res.* 198, 117132.

642 Zhou, L., Martin, S., Cheng, W., Lassabatere, L., Boily, J., Hanna, K., 2019. Water flow variability  
643 affects adsorption and oxidation of ciprofloxacin onto hematite. *Environ. Sci. Technol.* 53, 10102-  
644 10109.

645 Zhu, M., Paul, K.W., Kubicki, J.D., Sparks, D.L., 2009. Quantum Chemical Study of Arsenic (III, V)  
646 Adsorption on Mn-Oxides: Implications for Arsenic(III) Oxidation. *Environ. Sci. Technol.* 43,  
647 6655-6661.

648 Zhu, M., Ginder-Vogel, M., Parikh, S.J., Feng, X., Sparks, D.L., 2010. Cation Effects on the Layer  
649 Structure of Biogenic Mn-Oxides. *Environ. Sci. Technol.* 44, 4465-4471.

650